Influence of band gradients on Cu(In,Ga)Se2 solar cell diode factors

Thomas Orgis, Matthias Maiberg, and Roland Scheer

Citation: J. Appl. Phys. **114**, 214506 (2013); doi: 10.1063/1.4840995
View online: http://dx.doi.org/10.1063/1.4840995
View Table of Contents: http://jap.aip.org/resource/1/JAPIAU/v114/i21
Published by the AIP Publishing LLC.

Additional information on J. Appl. Phys.

Journal Homepage: http://jap.aip.org/
Journal Information: http://jap.aip.org/about/about_the_journal
Top downloads: http://jap.aip.org/features/most_downloaded
Information for Authors: http://jap.aip.org/authors

JOURNAL OF APPLIED PHYSICS **114**, 214506 (2013)

Influence of band gradients on Cu(In,Ga)Se_2 solar cell diode factors

Thomas Orgis,[a] Matthias Maiberg,[b] and Roland Scheer[c]
Martin Luther University Halle-Wittenberg, Fachgruppe Photovoltaik, Von-Danckelmann-Platz 3 06120 Halle (Saale), Germany

(Received 21 August 2013; accepted 19 November 2013; published online 6 December 2013)

The influence of band gap gradients on the charge collection and diode quality factor of solar cells is investigated by device simulation. A back surface band gap gradient manifested as a gradient of the conduction band is found to lead to an increased diode quality factor. Thus, the positive influence of the gradient on the fill factor is partially counterbalanced by the diode quality factor increase. The reason for the latter is the enhanced contribution of space charge region recombination. If the cell is equipped with a double gradient at front and back surfaces, the detrimental diode factor increase can be suppressed. The relevance of the findings is investigated using different carrier lifetimes and doping levels. © *2013 AIP Publishing LLC*. [http://dx.doi.org/10.1063/1.4840995]

I. INTRODUCTION

Recombination in heterostructure solar cells, being essentially p-n diodes, can take place at different sites: At the interfaces, in the space charge region (SCR) or in the quasi-neutral region (QNR). In fact, all recombination sites will be active in parallel.[1] However, in terms of limitation of open-circuit voltage V_{oc}, one of these mechanisms may be dominant. A means to elucidate this dominant recombination site is to determine the diode factor and activation energy of the diodes. This paper considers solar cells which, due to an appropriate conduction band alignment at the heterointerface, are immune against interface recombination and which are limited by bulk recombination.[2] Then, there are two possibilities: Either SCR recombination, which will show up with a diode factor near $A \approx 2$, or recombination in the QNR, which has $A \approx 1$, will dominate. In both cases, the activation energy of the saturation current density will equal the band gap energy.[1]

There are particular cases of SCR recombination where A systematically deviates from 2. Values of A larger than 2 can occur due to tunneling enhanced recombination,[3] recombination via coupled defects,[4] saturated donor-acceptor pair recombination,[5] or fluctuating band gap energies.[6] Values of A between 1 and 2 can occur for SCR recombination in the presence of an exponential distribution of defect energies in the band gap.[7] For larger lifetimes, i.e., for QNR recombination, A factors considerably larger than 1 cannot be explained so far.

The present work investigates the effect of a band gap gradient on the diode factor by device simulation. While the corresponding device model is implemented in 3D, effectively only 1D structures are employed, as the band gap gradient extends along one dimension only. Grain boundary effects are currently not considered. Simulations show that the grain boundary recombination velocity in efficient Cu(In,Ga)Se_2 (CIGS) solar cells is only in the range of 10^3 cm/s and thus small.[8] In addition, the diode quality factor was found to be unaffected if grain boundaries are within SCR and QNR.[9] Thus, the conclusions of the following study will be valid also in the presence of grain boundaries.

It turns out that for cells exhibiting high carrier lifetime ($\tau_{n0,p0} \geq 10$ ns) and a conduction band gradient towards the back contact the derived A factor near V_{oc} will be larger than 1, however, with a considerable voltage dependence. Such a large diode quality factor was reported for a champion CIGS laboratory solar cell with efficiency $\eta_{EC} = 20.3\%$ and $A = 1.4$.[10] As typical CIGS solar cells exhibit a band gap gradient due to a gradient in the Ga/(Ga + In) ratio, the simulations offer an explanation for the so far puzzling experimental results.

This study complements earlier simulation work on gradients in solar cell absorbers that focused on the possible efficiency gains compared to non-graded devices, considering the reduced back surface recombination[11] and also performance of combined front and back gradients.[12,13]

II. SIMULATION SETUP

The Synopsys® Sentaurus Advanced TCAD suite is employed to model an idealized CIGS cell with constant properties for the layers apart from the band gradient in the absorber. Contacts are Ohmic with fixed recombination velocities. The device is dominated by recombination inside the absorber bulk with minor contribution by the back contact, as recombination in window and buffer as well as at the heterointerface is intentionally excluded (i.e., corresponding to passivation via front gradient in valence band) and the back contact minority recombination velocity is set very low at $S_n = 100$ cm/s. Model parameters are shown in Table I, while Figure 1(a) represents the general band structure of the device. Volume recombination is treated via the Shockley-Read-Hall (SRH) model with constant carrier lifetime τ for both electrons and holes, corresponding to a mid-gap distribution of efficient recombination centers.

[a]Present address: Alfred Wegener Institute Potsdam, Telegrafenberg A43, 14473 Potsdam, Germany. Electronic mail: thomas@orgis.org
[b]Electronic mail: matthias.maiberg@physik.uni-halle.de
[c]Electronic mail: roland.scheer@physik.uni-halle.de

 © 2013 AIP Publishing LLC

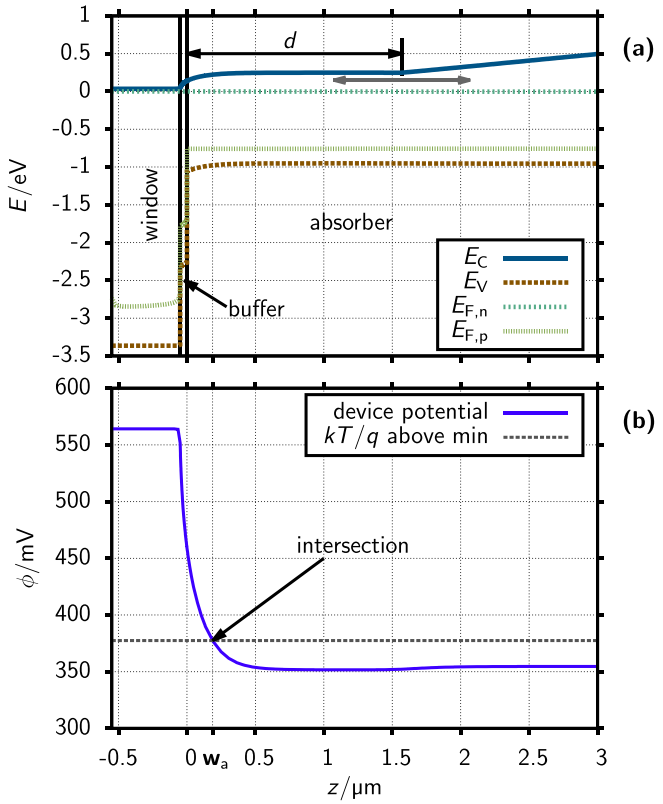

FIG. 1. (a) Device structure and band diagram, the three device layers (from left to right: window, buffer, absorber) being indicated in the band diagram via vertical lines and the onset point d (distance from interface) defining the extend of the conduction band gradient. (b) Electrostatic potential ϕ along z for determination of SCR width w_a, including the defining intersection with the level of kT/q above minimum. Lowdope case with $\tau = 100\,\text{ns}$, $d = 1.57\,\mu\text{m}$ and computed generation with $j_E = 100\,\text{mW/cm}^2$ at open circuit.

Doping and lifetime values are chosen according to the findings by Metzger *et al.*[8] and the standard CIGS device suggested by Scheer and Schock.[1]

Bandgap gradients are achieved via linear variation of modeled material composition within a single material layer, in contrast to stepped layers,[12,13] which in the chosen setup only affects resulting band gap and electron affinity. The absorption spectrum is fixed on a reference data set for CIS, the effect of increasing band gap on number of actually generated charge carriers being included in the runs denoted by "computed generation." Thus, with the bandgap monotonically increasing towards the back contact and absorption of reflected light from the back contact not being of concern here, the net result is similar to the approach of shifting the absorption edge, as performed by Gloeckler and Sites.[13]

Since this study focuses on the effects of the bandgap gradient on carrier collection and diode current, the main set of runs neglects the effect of gradients on generation by employing a fixed generation profile corresponding to zero gradient length, i.e., gradient onset $d = 3\,\mu\text{m}$. These data sets are labelled with "fixed generation" opposed to "computed generation."

The length of the conduction band gradient is varied and then characteristics are computed for a range of illumination intensities. One variation data set consists of current-voltage characteristics $j(V)$ for 20 gradients and 20 illumination intensities.

III. ANALYSIS

As we are interested in detectable device parameters as the outcome of a band gap gradient, we shortly give an overview of the analysis methods used to extract these parameters from the experimental data.

A. Basic *j(V)* characteristics

The basic solar cell parameters are taken from a single simulated $j(V)$ curve, using spline interpolation for enhanced accuracy where appropriate. The energy conversion efficiency η_{EC} is defined as the relation of the maximum power density extracted from the device, given via V_{mpp} and $j_{mpp} = j(V_{mpp})$, to the input illumination power density. j_{sc} is the absolute value of $j(0)$, V_{oc} the voltage with $j = 0$. Derived from those is the fill factor $FF = V_{mpp} j_{mpp}/(V_{oc} j_{oc})$.

B. Diode factor

In any diode model, the diode factor A is a parameter controlling the degree of voltage dependence of the current, i.e., the "steepness" of the $j(V)$ curve. It is related to the fill factor FF with the general trend of decreasing FF with increasing A. Without shunt and series resistances a single diode model is defined through the illuminated current equation

$$j(V) = j_0\left(\exp\left(\frac{qV}{AkT}\right) - 1\right) - j_{sc}\eta(V). \tag{1}$$

The diode factor can be calculated from a set of $j(V)$-curves with different illumination levels by evaluating corresponding V_{oc} and $j_{sc}\eta(V_{oc})$ values. With

$$j(V_{oc}) = 0 = j_0\left(\exp\left(\frac{qV_{oc}}{AkT}\right) - 1\right) - j_{sc}\eta(V_{oc}) \tag{2}$$

and the approximation

$$\exp\left(\frac{qV_{oc}}{AkT}\right) \gg 1 \Rightarrow \ln\frac{j_{sc}\eta(V_{oc})}{j_0} \approx \frac{q}{AkT}V_{oc} \tag{3}$$

the diode factor can be computed from the logarithmic slope

$$A \approx \frac{q}{kT}\left(\frac{\mathrm{d}}{\mathrm{d}V_{oc}}\ln\frac{j_{sc}\eta(V_{oc})}{j_0}\right)^{-1}. \tag{4}$$

At this point, we have implicitly assumed that a single diode model is sufficient to describe the current-voltage relation around V_{oc}, i.e., around the point of interest. Although this is a harsh simplification, we note that applying a one-diode model is common experimental practice for polycrystalline thin film diodes. An example of some plots of $\ln\left(j_{sc}\eta(V_{oc})/(\text{mA/cm}^{-2})\right)$ against V_{oc} in Figure 2 shows the changes in slope and hence diode factor for varying illumination. These changes might be non-trivial to diagnose for measured data that adds statistical errors. In consequence, one may interpret the $j(V)$ curve with a single diode model and may extract the relevant diode factor from the slope around V_{oc}.

TABLE I. Model parameters. If back surface grading is active, the absorber conduction band is raised by 0.25 eV towards the back contact, with varying length of graded region. For some simulations, front surface gradient of 0.125 eV is added. Interfaces are modeled defect-free with thermionic emission. Illumination for computed generation is specified by scaled AM1.5g spectra.

General parameter	Symbol/unit	Value		
Temperature	T/K	300		
n/p thermal velocity	$v_{\mathrm{th}}/(\mathrm{cm/s})$	1×10^{7}		
Volume parameter	**Symbol/unit**	**Window**	**Buffer**	**Absorber**
Depth	$d/\mu\mathrm{m}$	0.5	0.05	3
Electron affinity	χ/eV	4.3	4.3	4.3
Band gap	E_g/eV	3.4	2.4	1.2…1.45
Relative permittivity	ϵ	9	12	12
Electron mobility	$\mu_{\mathrm{n}}/(\mathrm{cm^2/V\,s})$	50	50	50
Hole mobility	$\mu_{\mathrm{p}}/(\mathrm{cm^2/V\,s})$	20	20	20
CB effective state density	$N_{\mathrm{C}}/\mathrm{cm^{-1}}$	4×10^{18}	2×10^{18}	2×10^{18}
VB effective state density	$N_{\mathrm{V}}/\mathrm{cm^{-1}}$	9×10^{18}	2×10^{19}	2×10^{18}
p doping	$N_{\mathrm{A}}/\mathrm{cm^{-3}}$			
“lowdope”		—	—	1×10^{15}
“normdope”		—	—	1×10^{16}
“highdope”		—	—	1×10^{17}
n doping	$N_{\mathrm{D}}/\mathrm{cm^{-3}}$	1×10^{18}	1×10^{15}	—
Radiative rec.	$C_{\mathrm{rad}}/\mathrm{s^{-1}}$	0	0	7.7×10^{-11}
SRH lifetime n/p	τ/ns	—	—	1, 10, 100
Contact parameter	**Symbol/unit**	**Front**	**Back**	
n surface recombination velocity	S_{n}/(cm/s)	1×10^{7}	1×10^{2}	
p surface recombination velocity	S_{p}/(cm/s)	1×10^{7}	1×10^{7}	

C. Collection efficiency and collection function

The external collection efficiency $\eta(V)$ needed here is estimated from the difference between $j(V)$ characteristics with differing illumination, denoted j_m and j_n,

$$\eta(V)\approx\frac{j_n(V)-j_m(V)}{j_{\mathrm{sc},n}-j_{\mathrm{sc},m}}. \tag{5}$$

In the ascending series of illumination intensities, the arithmetic mean of η with the previous and the next intensity in the series (if available) is used. The collection function is determined by a series of simulations that artificially increase carrier generation on grid nodes on top of the normal generation and measure both the resulting integral increase of generation in the discretized model domain and the corresponding integral increase in device current. In the case at hand with 3D setup and 1D structure, the computation of the collection function $\eta_{\mathrm{c}}(z)$ along z is achieved by selecting 2D slices sharing a z coordinate.

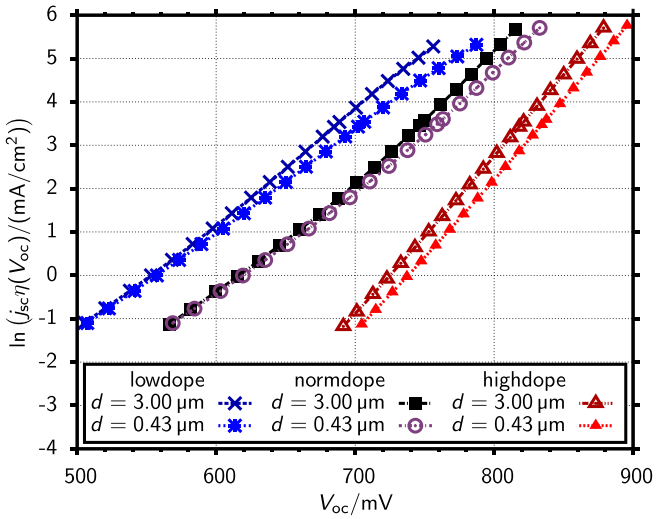

FIG. 2. Logarithm of $j_{\mathrm{sc}}\eta(V_{\mathrm{oc}})$ as a function of V_{oc} for graded cells ($d=0.43\,\mu$m) of different doping levels in comparison to non-graded cells ($d=3\,\mu$m). The non-constant slope determines the illumination-dependent diode factor. Case of computed generation with $\tau=10$ ns.

D. SCR and QNR

Having excluded other recombination channels, there remain two idealized contributions dominating the diode current: The currents due to SRH recombination in the SCR and in the QNR. Theory associates the QNR current with $A=1$ and the SCR current with $A=2$.

To distinguish the SCR region from the QNR region, a suitable definition of the SCR width w_{a} is needed, especially under illumination. The approach taken here defines the border of the space charge region at the point the electrostatic potential crosses the level of kT/q above the minimum (Figure 1(b)). The spatially integrated recombination rate in the SCR and QNR is computed from the simulated recombination profiles. Then, the quantity

$$r_{\mathrm{rec}}=\frac{\int_0^{w_{\mathrm{a}}}R(z)\mathrm{d}z}{\int_0^{w_{\mathrm{a}}}R(z)\mathrm{d}z+\int_{w_{\mathrm{a}}}^{d_{\mathrm{a}}}R(z)\mathrm{d}z} \tag{6}$$

is calculated, giving the ratio of SCR recombination over total recombination. This recombination index indicates dominance of SCR recombination for $r_{\mathrm{rec}} = 1$ and dominance of QNR recombination for $r_{\mathrm{rec}} = 0$. As laid out in by Scheer and Schock[1] (p. 59, without tunneling), this relation varies with changing carrier lifetimes due to the differing dependency of the respective reference current densities $j_{00,scr}$ and $j_{00,qnr}$ (and, by extension, $j_0 = j_{00}\exp(-E_a/AkT)$) on τ. It holds

$$j_{00,\mathrm{scr}} = \frac{kT}{F_m}\frac{\pi}{2}\left(\frac{N_C N_V}{\tau^2}\right)^{\frac{1}{A}} \overset{A=2}{\Rightarrow} j_{00,\mathrm{scr}} \sim \frac{1}{\tau} \tag{7}$$

and

$$j_{00,\mathrm{qnr}} = q\frac{D_n N_C N_V}{N_A}\underbrace{\frac{\mathrm{d}}{\mathrm{d}z}\eta_c(w_a)}_{\approx 1/L \sim 1/\sqrt{\tau}} \Rightarrow j_{00,\mathrm{qnr}} \sim \frac{1}{\sqrt{\tau}} \tag{8}$$

with densities of states N_C and N_V, electron diffusion coefficient D_n, field at maximum recombination F_m, and unit charge q. Hence, for increasing τ, $j_{00,scr}$ becomes more strongly reduced and r_{rec} shifts towards zero. In consequence, a shift of the diode factor towards $A = 1$ due to dominance of QNR recombination is expected. While the influence of τ and r_{rec} is clear, there is also a dependence on SCR widths and on bandgap gradients influencing the charge carrier collection.

IV. RESULTS AND DISCUSSION

In the following, we systematically vary the back surface gradient lengths for three different absorber doping levels ($N_A = 1\times10^{15}\,\mathrm{cm}^{-3}$, $1\times10^{16}\,\mathrm{cm}^{-3}$, and $1\times10^{17}\,\mathrm{cm}^{-3}$, subsequently referred to as "lowdope," "normdope," and "highdope," respectively). This will illustrate the differing influence of the SCR, due to its width strongly depending on the doping density. As carrier lifetime, we first chose 10 ns. Later, we also change the lifetime to 1 ns and 100 ns. Gradients are defined through the distance d of the gradient onset point from the buffer/absorber interface. Longer gradients are indicated by smaller d (Figure 1). At the end, we will also add a front surface gradient.

A. Gradient variation with normdope

The desired effect of a back surface bandgap gradient is to reduce recombination and enhance collection in the QNR—see analytic treatment by Green.[14] As shown in Figure 3(a), the collection function η_c in the QNR ($0.3\,\mu\mathrm{m} < z < 3\,\mu\mathrm{m}$) increases for decreasing d and saturates around $d \approx 0.3\,\mu$m. In addition, the external collection efficiency at the maximum power point $\eta(V_{\mathrm{mpp}})$ increases. As the collection function at point z gives the probability of a charge carrier generated at z to be collected, we expect an increase in short-circuit current with decreasing d. This is indeed evident in Figure 4(b), at least for $d > 0.7\,\mu$m. But also the open-circuit voltage increases in Figure 4(b). This becomes possible due to a decrease of $|\frac{\mathrm{d}}{\mathrm{d}z}\eta_c(z)|$, according to the reciprocity theorem for charge collection.[15] The fill factor exhibits a clear maximum at $d \approx 0.3\,\mu$m. The obvious negative effect of too long gradients is a smaller j_{sc} due to

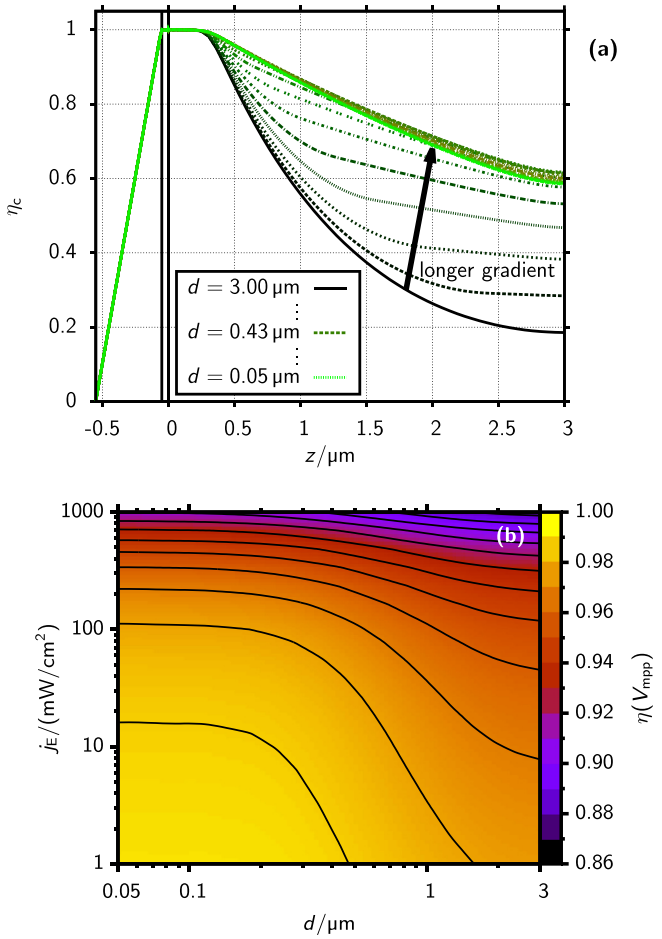

FIG. 3. (a) Collection function $\eta_c(z)$ at 100 mW/cm^2 for different onset d of back surface gradient. (b) Map of external collection $\eta(V_{\mathrm{mpp}})$ with varying back surface gradient and illumination (with contours corresponding to tick values on the color bar). Normdope case with $\tau = 10$ ns and computed generation).

reduced generation. When disregarding this effect of the widened bandgap by fixing the carrier generation to the case without gradient, one can analyze the electrical effects in isolation: As Figure 4(a) shows, the values of FF for computed and fixed generation are almost identical. The same is true for V_{oc}, where we see the effect of increasing effective band gap. Differences in η_{EC} between computed and fixed generation then are only a result of varying carrier density. This brings us to the point that we can discuss the FF effect as the major factor determining the maximum of η_{EC} for the (realistic) case of computed generation. In accordance with other studies,[13] we find that an optimum gradient extends from the end of the space charge region to the back contact.

The new aspect presented in this study is the comparison of the diode factors derived at V_{oc}. Here, we consider the case of computed generation, which shows the same behavior as the fixed generation case. The map of diode factors for different gradients and illumination levels is represented in Figure 5(c). The diode factor changes in a range from about 1.2 to 1.8. It generally increases with gradient length and decreases with illumination power density. Together with the collection efficiency, the diode factor has a distinct influence on FF. We may verify this by seeking an analytical expression of $FF(\eta(V_{\mathrm{mpp}}), A)$. From the relation Eq. (1), we calculate $FF(\eta(V_{\mathrm{mpp}}), A)$ in the limit of the approximations

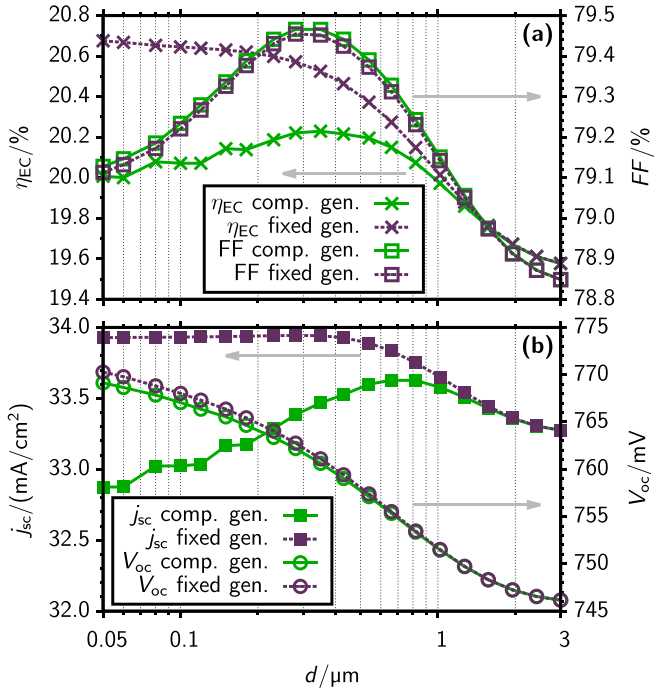

FIG. 4. Solar cell parameters for simulation run with computed generation compared to fixed generation depending on back surface gradient onset d, for normdope with $\tau = 10\,\mathrm{ns}$ at $j_E = 100\,\mathrm{mW/cm^2}$, showing η_{EC} and FF in (a) and j_{sc} and V_{oc} in (b).

$$\left(\frac{\mathrm{d}}{\mathrm{d}V}\eta\right)_{mpp} \approx 0, \quad \eta(V_{oc}) \approx \eta(V_{mpp}) \tag{9}$$

and

$$\ln\left(1+\frac{qV_{mpp}}{AkT}\right) \approx \ln\left(1+\frac{qV_{oc}}{AkT}\right) \tag{10}$$

and obtain

$$FF = \eta(V_{mpp})\frac{\frac{qV_{oc}}{AkT} - \ln\left(\frac{qV_{oc}}{AkT}+1\right)}{\frac{qV_{oc}}{AkT}+1}. \tag{11}$$

Thus, the collection efficiency modifies the expression for the ideal FF.[16] A higher $\eta(V_{mpp})$ gives rise to a larger FF. Equation (11) can be further simplified for $\frac{qV_{oc}}{AkT} \gg 1$ to

$$FF \approx \eta(V_{mpp})\left(1 - \frac{AkT}{qV_{oc}}\ln\left(\frac{qV_{oc}}{AkT}\right)\right), \tag{12}$$

showing a quasi-linear negative dependence of FF on A.

Now, looking at the diode factor in Figure 5(c) at the cut of $j_E = 100\,\mathrm{mW/cm^2}$ and the collection efficiency in Figure 3, we find the reason for the distinct maximum of FF in Figure 4(a) in the variation of A and $\eta(V)$: For a too long gradient, the gain in collection is counterbalanced by the

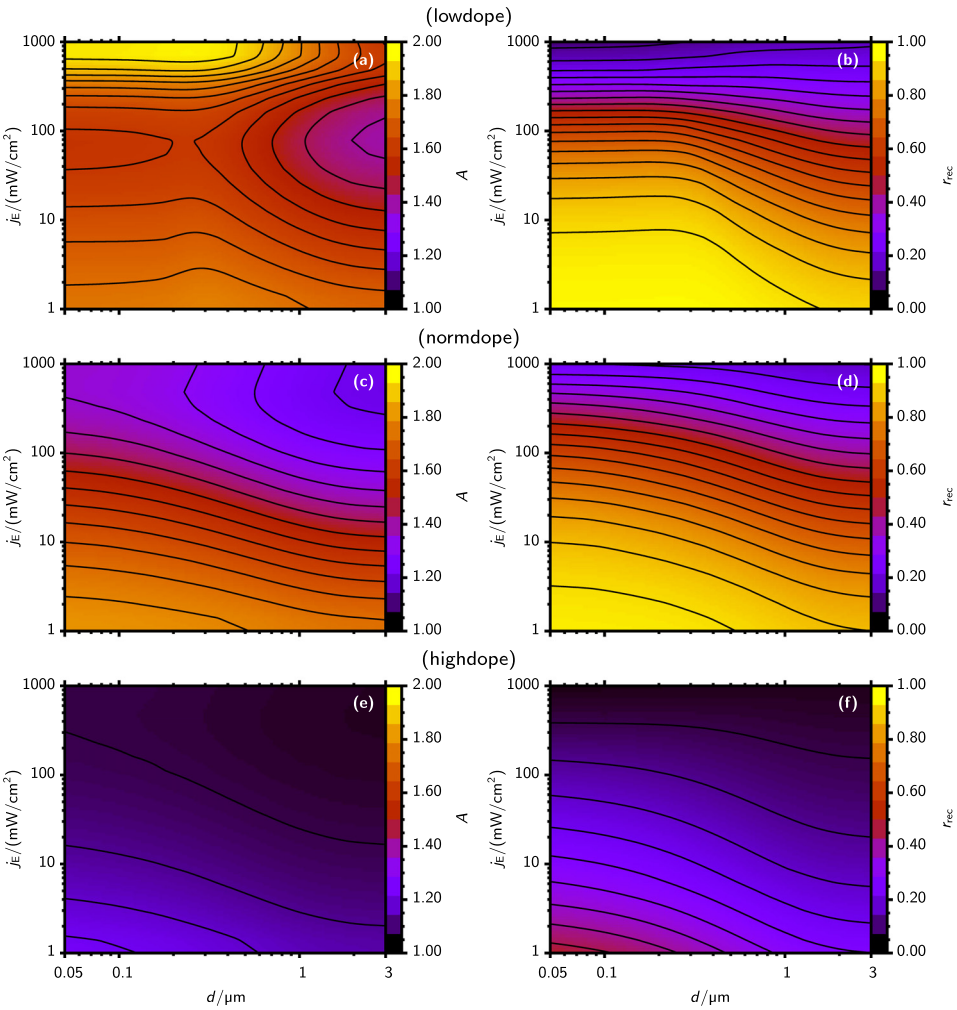

FIG. 5. Parameter maps for diode factor A ((a), (c), (e)) and recombination index r_{rec} ((b), (d), (f)) for the runs with $\tau = 10\,\mathrm{ns}$, with low ((a), (b)), normal ((c), (d)) and high ((e), (f)) doping, each covering differing gradients onsets d and illumination j_E. Shown case is fixed generation, diode factor being practically identical to computed generation case. Contours correspond to tick values on the respective color bar.

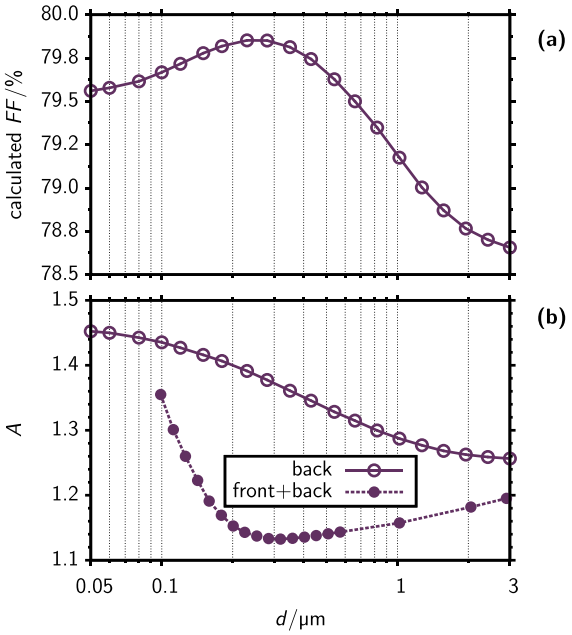

FIG. 6. (a) Calculated values of FF for a back surface gradient according to Eq. (11) using simulated values of A and $\eta(V_{mpp})$. (b) Diode factors for a simple back surface gradient (full line with circles) from Figure 5(c) (cut at 100 mW/cm^2) and for combined front and back surface gradients (dashed line with filled circles) as a function of gradient onset d.

increasing diode factor (Figure 6(b)). Despite a small offset, the calculated FF shown in Figure 6(a) resembles the general trend of the measured FF.

In order to understand the diode factor increase with the gradient length, we consider the recombination index as a function of d in Figure 5: Obviously, r_{rec} becomes larger for smaller d. There is a significant decrease in QNR recombination and, correspondingly, an increase in SCR recombination with smaller d. Now, a shift towards dominance of SCR recombination means higher diode factors.

The correlation between A and r_{rec} is also generally apparent in the normdope scatterplot of Figure 7(d). In a scatterplot, clustering of data points along a straight line indicates a linear relation between the parameters under investigation. For intermediate values of A and r_{rec} there is a strong correlation in Figure 7(d), so that for the case of normal doping with $\tau = 10$ ns, the recombination index is the main parameter explaining the variation of diode factor. But systematic drift of the points especially with high illumination power density is also visible.

B. Different doping densities (changing SCR width)

Further simulations explore if the correlation between r_{rec} and A also holds for other absorber doping, thereby

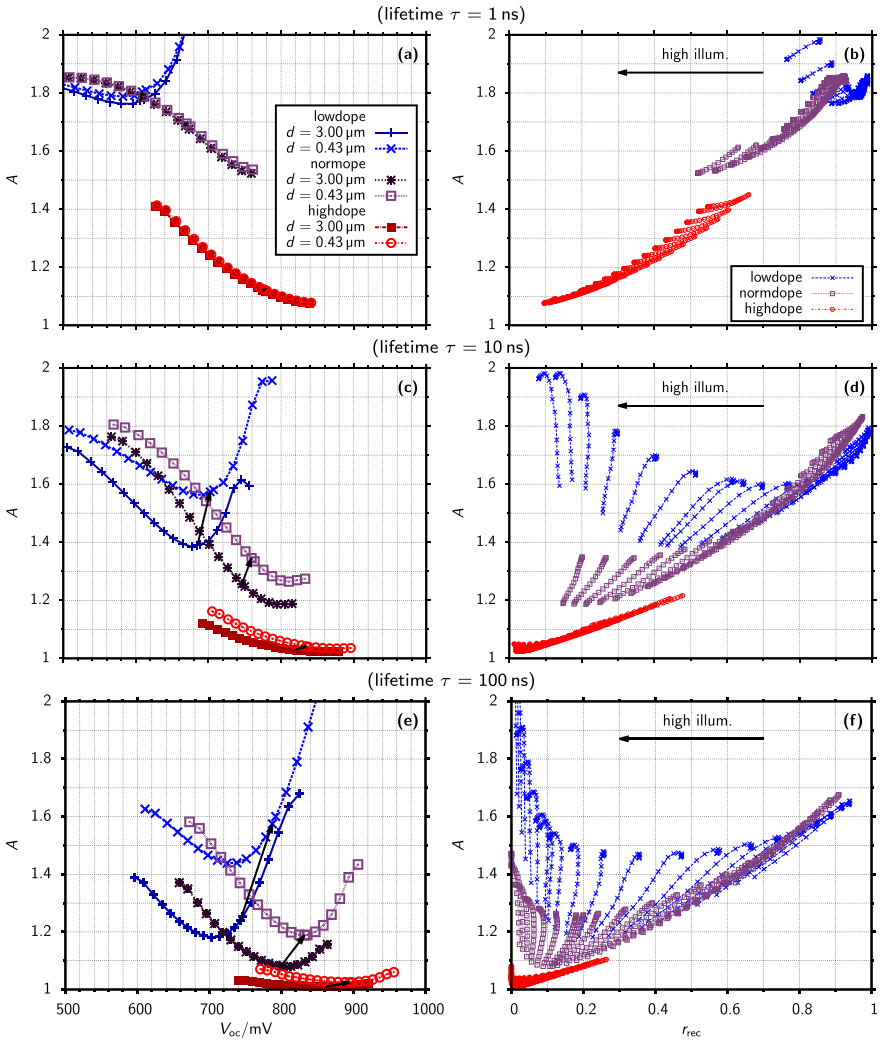

FIG. 7. Case of back surface gradient and fixed generation. Left ((a), (c), (e)): Diode factors depending on V_{oc} (due to corresponding illumination) for the three doping cases, with and without gradients, for carrier life time of 1 ns (a), 10 ns (c) and 100 ns (e). Right ((b), (d), (f)): Correlation scatterplots for A and r_{rec}, for the same data sets and lifetimes, but covering all computed gradients. Connected dots share the illumination level, the arrow indicating the general direction towards higher illumination.

modifying the width of the SCR. With the normdope case of $N_A = 1 \times 10^{16}\,\mathrm{cm}^{-3}$, the SCR width is $w_a \approx 0.1\,\mu\mathrm{m}$ at one sun ($j_E = 100\,\mathrm{mW/cm}^2$). When increasing the doping to $N_A = 1 \times 10^{17}\,\mathrm{cm}^{-3}$, the width reduces to $w_a \approx 0.015\,\mu\mathrm{m}$, while a decrease of the doping to $N_A = 1 \times 10^{15}\,\mathrm{cm}^{-3}$ prompts larger $w_a \approx 0.32\,\mu\mathrm{m}$. The actual volume available for SCR recombination limits the impact a gradient can exert on the diode factor. In the case of high doping density and small SCR width w_a (Figures 5(e) and 5(f)), the diode factor only varies below 1.2, that variation also being largely explained by the recombination index (Figure 7(b)). This device is clearly dominated by QNR recombination and changes in relative recombination strength are small.

With lowered doping density and a wider SCR, a generally higher diode factor is expected. This is evident in Figures 5(a) and 5(b), but the relation to r_{rec} is not that clear. For low illumination, r_{rec} and A agree well, but for higher light intensities, A changes independently of r_{rec}. The diode factor starts to rise with higher illumination, after falling towards one sun. This can be explained by the excess hole density which becomes comparable to the doping density. Under powerful illumination and with sufficiently low doping, both electron and hole densities start to vary with illumination (and hence rising OC voltage) also in the QNR (hole quasi Fermi level varies), and hence the recombination in the QNR actually changes character, approaching diode factor 2. This explains the disturbed correlation in the scatterplot in Figure 7(d), corresponding to Figures 5(a) and 5(b).

C. Overview with differing lifetimes

Finally, the carrier lifetime τ is varied. Runs with $\tau = 1$ ns, 10 ns, and 100 ns for three doping regimes are represented in Figure 7. We compare the diode factor dependence on V_{oc} without gradient (d3.00, $d = 3\,\mu\mathrm{m}$) and with effective gradient (d0.43, $d = 0.43\,\mu\mathrm{m}$) on the left side (a, c, e) and show on the right (b, d, f) the correlation between recombination index and diode factor for the whole parameter space (gradients and illuminations) in scatterplots.

As a general trend, the diode factor decreases with V_{oc} exhibiting the transition from SCR to QNR recombination. That slope saturates at some point and, especially for low doping, a raise of diode factor can be discerned after that.

This overview shows that increasing lifetime, by enhancing QNR recombination relative to SCR, generally shifts the diode factor towards 1, matching the expectation noted before. For very low lifetime, there is barely any effect of the bandgap gradient on the diode factor, while with high lifetimes, the increase in diode factor is very pronounced for low and normal doping densities, consistent with the more prominent role of QNR recombination, in accordance with Eqs. (7) and (8). Whatever variation of diode factor there is, it is generally well correlated to the change in recombination index, but decreasingly so for lower doping because of the excess hole densities in the QNR becoming significant at high voltages, as discussed before. This effect scales with the doping density, peaking in the upwards turn of A over V_{oc} for low doping or high lifetime, but also being noticeable at normal and high doping densities and lower lifetimes.

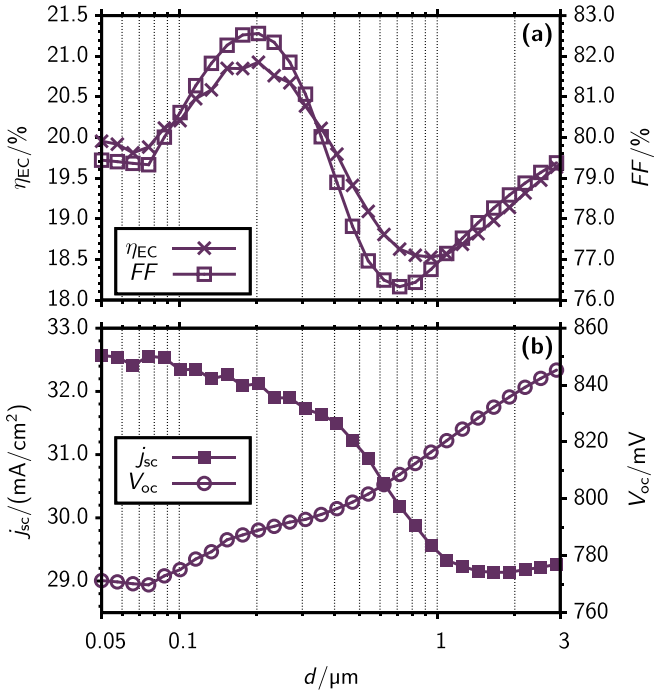

FIG. 8. Solar cell parameters for simulation run with combined front and back surface gradient depending on gradient onset d, for normdope with $\tau = 10$ ns at $j_E = 100\,\mathrm{mW/cm}^2$ (compare Figure 4), showing η_{EC} and FF in (a) and j_{sc} and V_{oc} in (b). Case of computed generation.

D. Influence of combined back and front surface gradients

In response to the observed non-optimum effect of a simple back surface gradient with the drawback of increased SCR recombination, one can use combined back and front surface gradients.[12,13] Here, we select a front surface gradient (0.125 eV) having a height 50% of the back surface gradient (0.25 eV). This gives an asymmetric V-shaped profile of the conduction band edge now with onset d of both gradients (notch point). Again, we investigate the effect of d on the solar cell parameters and chose the computed generation case. In Figure 8, we find a maximum efficiency with a notch point at 0.2 μm, which is near the SCR boundary.

The maximum in η_{EC} is again due to a maximum in FF, while the effects on V_{oc} and J_{sc} largely compensate each other. Beyond the optimum d point, the efficiency severely drops to a value below that of the non-graded reference cell (see sample with $d = 3\,\mu\mathrm{m}$ in Figure 4). However, the maximum efficiency exceeds the simple back contact case. This is mainly due to a reduction of SCR recombination as underlined by the reduced diode factor in Figure 6(b).

V. CONCLUSIONS

This investigation complements earlier work concerned with the net effect on efficiency exerted by bandgap back surface gradients, by analyzing the resulting diode factor at open circuit and related parameters. Depending on doping density and lifetime, there can be a significant effect of the gradient on diode factor, namely an increase of A by decreasing the QNR recombination. As long as high injection does not change the character of QNR recombination, the changes in diode factor can be simply traced back to the relative

strength of SCR recombination ($A = 2$) relative to QNR recombination ($A = 1$), embodied in the recombination index r_{rec} ($r_{rec} = 0$ for total QNR domination, $r_{rec} = 1$ for SCR).

There is a combination of the efficiency-enhancing effect of improved collection and hence increased V_{oc} and j_{sc} and a shift towards higher A factors. It follows that, for instance, if a highly efficient CIGS solar cell is dominated by bulk recombination in the absorber and features a Ga gradient giving rise to a bandgap back surface gradient like investigated here (qualitative agreement with experimental works),[17,18] it is bound to have a diode factor significantly larger than 1, as observed by Jackson *et al.*[10] This increased diode factor is responsible for partial out-balancing of the increase of the fill factor by the enhanced collection, which matches the relatively low fill factor observed by Jackson *et al.*[10] The detrimental diode factor effect can be largely circumvented by a combination of back and front surface gradients.

The study of the characteristics for different doping densities and carrier lifetimes confirms theoretical expectations about scaling of gradient influence with SCR width as well as diode factor shifts with lifetime, and also the more complex behavior when approaching high-injection regimes.

ACKNOWLEDGMENTS

This work has been supported by the BMBF project GRACIS (03SF0359H). We thank the anonymous reviewer for the helpful comments.

[1]R. Scheer and H. Schock, *Chalcogenide Photovoltaics* (WILEY-VCH, Weinheim, Germany, 2011).
[2]R. Scheer, J. Appl. Phys. **105**, 104505 (2009).
[3]U. Rau, Appl. Phys. Lett. **74**, 111 (1999).
[4]A. Schenk and U. Krumbein, J. Appl. Phys. **78**, 3185 (1995).
[5]O. Breitenstein, P. Altermatt, K. Ramspeck, M. Green, J. Zhao, and A. Schenk, in Proceedings of the 4th World Photovoltaic Solar Energy Conference (IEEE, 2006), p. 879.
[6]J. Werner, J. Mattheis, and U. Rau, Thin Solid Films **480–481**, 399 (2005).
[7]T. Walter, R. Herberholz, and H. Schock, Solid State Phenom. **51–52**, 309 (1996).
[8]W. Metzger, I. Repins, M. Romero, P. Dippo, M. Contreras, R. Noufi, and D. Levi, Thin Solid Films **517**, 2360 (2009).
[9]M. Gloeckler, J. R. Sites, and W. K. Metzger, J. Appl. Phys. **98**, 113704 (2005).
[10]P. Jackson, D. Hariskos, E. Lotter, S. Paete, R. Wuerz, R. Menner, W. Wischmann, and M. Powalla, Prog. Photovoltaics **19**, 894 (2011).
[11]T. Dullweber, O. Lundberg, J. Malmström, M. Bodegård, L. Stolt, U. Rau, H. Schock, and J. Werner, Thin Solid Films **387**, 11 (2001).
[12]J. Song, S. S. Li, C. Huang, O. Crisalle, and T. Anderson, Solid-State Electron. **48**, 73 (2004).
[13]M. Gloeckler and J. Sites, J. Phys. Chem. Solid **66**, 1891 (2005).
[14]M. Green, Prog. Photovoltaics **17**, 57 (2009).
[15]C. Donolato, J. Appl. Phys. **66**, 4524 (1989).
[16]A. de Vos, Sol. Cells **8**, 283 (1983).
[17]G. Bauer, S. Heise, S. Knabe, O. Neumann, R. Brüggemann, D. Hariskos, and W. Witte, Energy Proc. **10**, 208 (2011).
[18]W. Witte, M. Powalla, D. Hariskos, A. Eicke, M. Botros, W. H.-Schock, D. Abou-Ras, R. Mainz, H. Rodríguez-Alvarez, T. Unold, G. Bauer, R. Brüggemann, S. Heise, O. Neumann, M. Meessen, J. Christen, F. Bertram, M. Müller, A. Klein, T. Adler, K. Albe, J. Pohl, M. Martin, R. De Souza, L. Nagarajan, T. Beckers, C. Boit, J. Dietrich, M. Hetterich, Z. Zhang, R. Scheer, H. Kempa, and T. Orgis, in *Proceedings 27th European Photovoltaic Solar Energy Conference, EU PVSEC* (WIP Munich, Munich, 2012), p. 2166.